Journal of Molecular Catalysis A: Chemical 338 (2011) 24–32

Contents lists available at ScienceDirect

Journal of Molecular Catalysis A: Chemical

journal homepage: www.elsevier.com/locate/molcata

A DFT study on the distributions of Al and Brönsted acid sites in zeolite MCM-22

Yan Li[a,b], Wenping Guo[c], Weibin Fan[a,*], Shuping Yuan[a,d], Junfen Li[a], Jianguo Wang[a,*], Haijun Jiao[a,e,**], Takashi Tatsumi[f]

[a] State Key Laboratory of Coal Conversion, Institute of Coal Chemistry, Chinese Academy of Sciences, 27 South Taoyuan Road, Taiyuan 030001, China
[b] Graduate University of Chinese Academy of Sciences, Beijing 100049, China
[c] State Key Laboratory for Physical Chemistry of Solid Surfaces and Department of Chemistry, College of Chemistry and Chemical Engineering, Xiamen University, Xiamen 361005, China
[d] Institute for Computational Science and Engineering, Laboratory of New Fibrous Materials and Modern Textile, the Growing Base for State Key Laboratory, Qingdao University, Qingdao 266071, China
[e] Leibniz-Institut für Katalyse e.V. an der Universität Rostock, Albert-Einstein-Strasse 29a, 18059 Rostock, Germany
[f] Catalytic Chemistry Division, Chemical Resources Laboratory, Tokyo Institute of Technology, Nagatsuta 4259, Midori-ku, Yokohama 226-8503, Japan

ARTICLE INFO

Article history:
Received 15 November 2010
Received in revised form 10 January 2011
Accepted 18 January 2011
Available online 27 January 2011

Keywords:
Density functional theory
ONIOM method
MCM-22
Brönsted acid
Zeolite

ABSTRACT

Density functional theory (DFT) calculations were employed to investigate the positions of Al in the framework of Na-MCM-22 as well as the locations and strengths of Brönsted acid sites in the corresponding H-MCM-22 analogue. Thermodynamically, the most favorable sites for locating Al are T7 and T1 sites, followed by T5, T3 and T4, while T2, T8 and T6 sites are unlikely to be occupied because of less stability. Accordingly, two types of Si(OH)Al groups, viz. isolated and H-bonded bridging OH species, were found in H-MCM-22. This finding is supported by the perfect agreement between the calculated and experimentally observed OH vibrational frequencies. The calibrated N_2 and CO adsorption energies on the bridging OH sites reveal stronger Brönsted acidity of Al3–O13H–Si3 and Al4–O7H–Si4 sites than Al1–O3H–Si4 and Al3–O12H–Si3 sites.

1. Introduction

Zeolites are microporous crystalline aluminosilicates widely used as adsorbents and catalysts in petrochemical and fine chemical industry [1]. The adsorptive and catalytic properties of zeolites depended on their structures as well as the locations and strengths of acid sites, which are determined by the Al amounts and distributions in their frameworks.

MCM-22 possesses a unique layered structure (MWW structure) with two independent 10-membered ring (10-MR) pore systems, viz. the intralayer 2D sinusoidal channel and the interlayer pore opening connected to 12-MR supercages (1.8 nm × 1.8 nm × 0.72 nm) [2]. This material has been proved to be catalytically active for many reactions such as alkylation of benzene and cracking of *n*-alkanes. It is also used as an FCC octane booster additive especially valuable for the production of reformulated gasolines [3].

Eight crystallographically non-equivalent lattice sites are present in the framework of MCM-22. The distribution of Al in these sites, being dependent on the Al content and synthesis conditions [4–7], strongly influences the catalytic properties. For alkylation of toluene with propene over H-MCM-22, the reaction only occurs in the external side pockets (hemicages), while the Brönsted acid sites in the supercages and sinusoidal channels mainly produce coke and C_4–C_6 alkenes, respectively [8]. In contrast, in the case of methanol-to-olefin (MTO) reaction, the Brönsted acid sites in the sinusoidal channels contribute much more to the overall MTO performance than those in the supercages and external side pockets [9].

Thus, many authors have directed their efforts to study the distributions of Al and Brönsted acid sites in the framework of MCM-22 by using FTIR and MAS NMR spectroscopies in combination with the adsorption of different-sized basic probe molecules such as nitriles [5,10–13]. ^{27}Al MAS NMR spectroscopy shows that at least three types of tetrahedral Al species are present in MCM-22 due to Al occupying in the crystallographically different lattice sites [12]. Based on the measured IR spectra, Góra-Marek and Datka [6] suggested that Al inserted in both the supercages and the intralayer 10-MR sinusoidal channels for the high silica MCM-22, an increase in the Al content resulting in the incorporation of Al mainly in the supercages.

* Corresponding authors. Tel.: +86 351 4046092; fax: +86 351 4041153.
** Corresponding author at: Leibniz-Institut für Katalyse e.V. an der Universität Rostock, Albert-Einstein-Strasse 29a, 18059 Rostock, Germany.
Tel: +49 381 1281 135; fax: +49 381 1281 5000.
E-mail addresses: fanwb@sxicc.ac.cn (W. Fan), iccjgwang@sxicc.ac.cn (J. Wang), haijun.jiao@catalysis.de (H. Jiao).

1381-1169/$ – see front matter © 2011 Elsevier B.V. All rights reserved.
doi:10.1016/j.molcata.2011.01.018

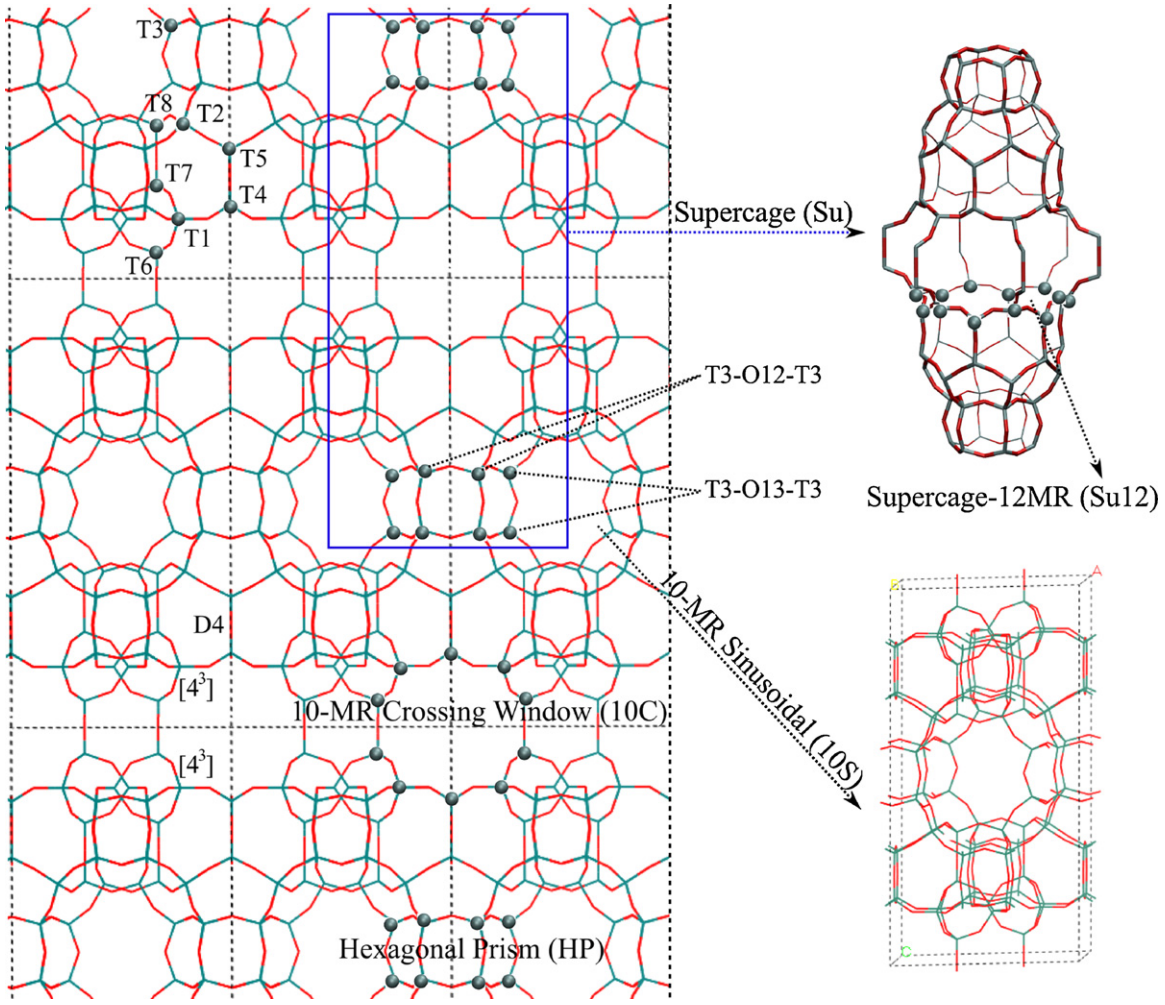

Fig. 1. Schemes for MCM-22 structure with 8 crystallographically inequivalent T sites and possible locations of Na^+ cations.

Since the location of Al in the framework of MCM-22 cannot be accurately determined by the present experimental techniques, theoretical calculations have been employed to reveal the preferential sites for Al occupation [14–18]. Due to the computation demanding, up to date only small cluster models (8T and 22T) have been used in high quality quantum mechanical calculations [17,18]. However, these studies gave significantly discrepant results [19]. In particular, the Al distribution in the framework obtained by assuming H^+ as charge-compensating ion in the 8T and 22T models [17,18] is not in line with the synthesis of MCM-22 usually with Na^+ as counter-ion [4,20]. According to the Pauling's rule, monovalent cations would interact with oxygen atoms attached to framework Al atoms [21]. Simoncic and Armbruster reported that a synergetic effect might exist between alkali metal ions and (Al,Si) order during crystal growth [22]. Thus, alkali metal ions in the framework would be closely correlated to the locations of Al in the lattice sites [23,24]. This has been confirmed by the effect of Na^+ on the distribution of Al in the framework of MOR zeolite [25]. Therefore, to reliably study the Al distribution in the framework of MCM-22, we have to build large cluster models with Na^+ as counter-ion and make efforts to setup an accurate and efficient methodology to reveal the locations of Al in the lattice sites [19].

In this context, the ONIOM method is employed here to investigate the distribution of Al in the framework of Na-MCM-22, and subsequently the locations and strengths of Brönsted acid sites in H-MCM-22.

2. Models and methods

Density functional theory (DFT) calculations were conducted on the basis of the refined hexagonal *P*6/*mmm* structure of pure silica MCM-22 [2], in which one unit cell includes eight crystallographically non-equivalent T sites (lattice sites). These T sites were labeled here according to Ref. [26] (Figs. 1 and 2). It was assumed that Al^{3+} would possibly occupy all of these T sites and the generated one negative charge was balanced by one Na^+ or one H^+. Consequently, two types of models, viz. Na-MCM-22 and H-MCM-22, were obtained. The preferential T sites for incorporating Al were determined by the substitution energy (*SE*) [18,27], which was defined as the reaction energy of the virtual reaction of $(Si–O–Si)_{cluster} + Al(OH)_3 + NaOH \rightarrow (Al–ONa–Si)_{cluster} + Si(OH)_4$ or of the reaction of $(Si–O–Si)_{cluster} + Al(OH)_3 + H_2O \rightarrow (Al–OH–Si)_{cluster} + Si(OH)_4$.

The *SE* was calculated in terms of the following Eq. (1) or (2). A lower *SE* is corresponding to a more stable substitution site.

$$SE(Al, Na) = E((Al–ONa–Si)_{cluster}) + E(Si(OH)_4) - E((Si–O–Si)_{cluster}) - E(Al(OH)_3) - E(NaOH) \quad (1)$$

$$SE(Al, H) = E((Al–OH–Si)_{cluster}) + E(Si(OH)_4) - E((Si–O–Si)_{cluster}) - E(Al(OH)_3) - E(H_2O) \quad (2)$$

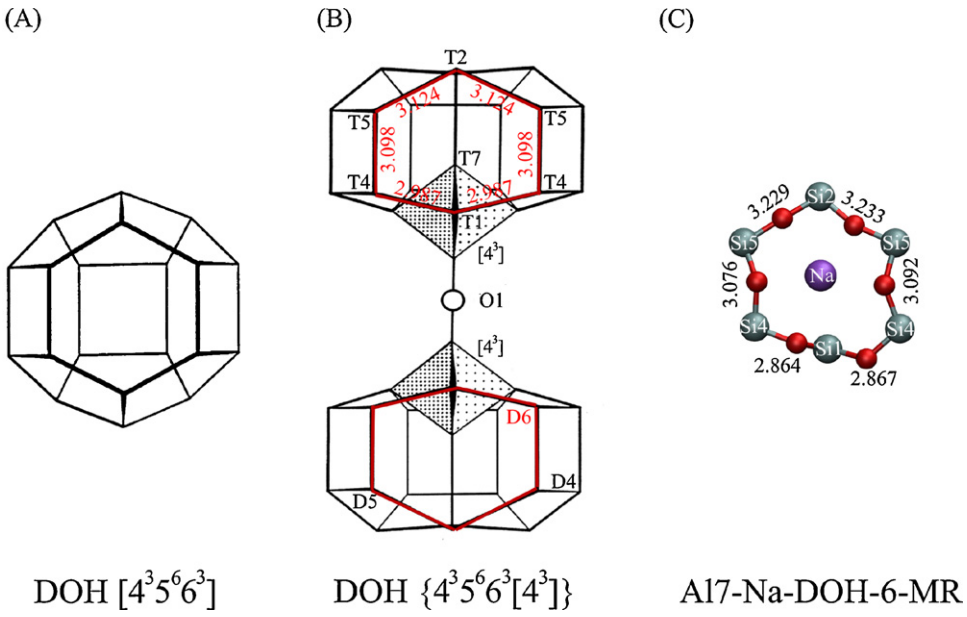

Fig. 2. Schemes for (A) $[4^3 5^6 6^3]$ (DOH) cage in dodecasil-1H, with idealized D_{3h} symmetry; (B) $\{4^3 5^6 6^3 [4^3]\}$ (modified DOH) cage in MCM-22, with idealized C_{3v} symmetry; (C) the distance of Si···Si in the 6-MR of the modified DOH cage from the optimized Al7-Na structure.

It was reported that the results calculated by the cluster model could be consistent with that obtained by the full periodic DFT calculations if the inner layer of the cluster includes all of the oxygen atoms which might be involved in the local interaction of the guest molecule with the zeolite framework [28]. The ONIOM method is employed here to model MCM-22 structure with a cluster large enough to satisfy such a prerequisite. For Na-MCM-22, the cluster models centered at each of the eight crystallographically inequivalent T sites were built with a radius of about 10 Å, being correspondent to 72T–116T clusters. Two-layer ONIOM scheme was applied, in which the high-layer regions cover 19–27 T sites with the centers at the corresponding T sites so that all the possible atoms for accommodation of Na^+ ions could be included. In the H-MCM-22 models, three-layer ONIOM scheme was established as the method reported in our previous paper [19]. For all the cluster models, the dangling Si atoms were terminated with H along the bond direction of the next lattice oxygen with the Si–H distance fixed at 1.47 Å. During the optimizations, only the terminal SiH_n (n = 1–3) groups were frozen.

All the calculations were carried out by the Gaussian 03 program package [29]. For Na-MCM-22, the structures were relaxed at ONIOM2 (B3LYP/6-31G(d):MNDO) level to determine the optimal locations of Na^+, and the final energies were calibrated by ONIOM2 (B3LYP/6-31G(d):HF/3-21G(d)) single point calculations on the optimized geometries [28]. For H-MCM-22, the structures were optimized at ONIOM3 (B3LYP/6-311G(d,p):HF/3-21G(d):MNDO) level, while the energies were improved at ONIOM2 (B3LYP/6-311G(d,p):HF/3-21G(d)) level by extending ONIOM3 medium layer to the whole system. The harmonic vibration frequencies of the bridging OH species were calculated at B3LYP/6-311G(d,p) with 8T cluster models cut from the optimized H-MCM-22 structures. The frequencies were obtained by using the ONIOM3 (B3LYP/6-311G(d,p):HF/3-21G(d):MNDO) method with anharmonicity corrections, as done in our pervious work [19]. The standard deviation in energy from the fitting of the Morse potentials is less than 0.08 kJ/mol, which corresponds to 6 cm^{-1}.

3. Results and discussion

3.1. Distribution of Al in the framework of Na-MCM-22

As well known, MCM-22 is usually synthesized in the presence of Na^+ ion, while it is very hard or impossible to be obtained with H^+ as counter-ion. Therefore, it is much more reasonable to inves-

Table 1
Calculated SE(Al,Na) (kJ mol^{-1}) and $SE(Al,Na)_{rel}$ (the substitution energy relative to that of Al7-Na/D6, kJ mol^{-1}) of Al for Si, CN and stable positions of Na^+, and distances of Na^+-oxygen (Å) in Na-MCM-22.

Al site	Models	SE(Al,Na)	$SE(Al,Na)_{rel}$	CN	Interacting T sites[a]	$r(Na^+\cdots O)$[b]	Positions
Al7–Na/D6	21T:89T	−456.8	0.0	6	[(2–5–4–1–4–5)+1–7^{Al}][c]	2.39 2.30 3.46 2.57 2.28 2.63 *2.45*	D6
Al1–Na/D6	21T:89T	−452.9	3.9	6	(2–5–4–1^{Al}–4–5)+1^{Al}–7	2.55 2.29 *3.52 2.36* 2.39 2.56 *2.56*	D6
Al5–Na/D6	26T:116T	−434.1	22.7	4	(2–5–4–1–4–5^{Al})+1–7	3.14 2.41 3.60 2.49 *2.36 2.27* 2.97	D6
Al3–Na/HP6	19T:114T	−433.7	23.0	4	(3–3–3–3–3^{Al}–3)	2.30 2.38 3.63 *2.35 2.19* 3.80	HP6
Al4–Na/D6	26T:83T	−431.3	25.5	3	(2–5–4–1–4^{Al}–5)+1–7	2.40 2.92 2.44 *3.25 2.23* 3.60 3.13	D6
Al2–Na/D6	27T:110T	−421.1	35.6	5	(2^{Al}–5–4–1–4–5)+1–7	*2.63* 2.32 3.67 2.52 2.68 *2.30* 3.13	D6
Al8–Na/10S	22T:114T	−414.2	42.5	2	[8^{Al}–2+8^{Al}–2+8^{Al}–2][d]	*2.25 2.32 3.43*	10S
Al6–Na/10C	16T:72T	−412.6	44.2	4	4–1–6^{Al}–6–1	2.54 *2.36 2.45* 2.51	10C

[a] T sites adjacent to oxygen atoms interacted with Na^+.
[b] The $r(Na^+\cdots O)$ written in italics represents the distances between Na^+ and oxygen atoms of AlO_4 tetrahedron. The distances are shown in the order corresponding to the specification given in the sixth column.
[c] The parentheses represent that six T sites consisted of a 6-MR with the ordering of T sites along the clockwise direction, as shown in Fig. 3. "+1–7" denotes T1 and T7 sites adjacent to oxygen atoms coordinated to Na^+ (T1 is located in the 6-MR but T7 is not, as shown in Fig. 3).
[d] One T8 site was adjacent to three oxygen atoms coordinated to Na^+ and each oxygen atom was adjacent to one T2 site.

tigate the locations of Al in its framework by using Na^+ instead of H^+ as the charge-compensating ion despite that Na^+ is probably present in the form of aqua complex in the crystalline gel, which may play a strong structure-forming role in the crystallization of MCM-22 [30,31]. In the framework of Na-MCM-22, a number of positions, such as 12-MR supercages, intralayer 10-MR sinusoidal channels (10S), 10-MR crossing windows (10C) or pore openings between layers and hexagonal prisms between supercages, could be occupied by Na^+ ion, as shown in Figs. 1 and 2. Su and Su12 refer to the sitings inside the supercages and at the 12-MR of the supercages respectively, whereas HP and HP6 represent the positions inside the hexagonal prism between supercages and at the 6-MR of the HP respectively. The Na^+ ion might be also located inside the $\{4^3 5^6 6^3 [4^3]\}$ cage. This cage is composed of 4-, 5- and 6-membered rings. Thus, there would be three types of sites, designated as DOH-4-MR (D4), DOH-5-MR (D5) and DOH-6-MR (D6), respectively, for locating Na^+. All the possible locations and coordination states of Na^+ ions in Na-MCM-22 were determined by assuming that Al could occupy each of the eight crystallographically non-equivalent T sites.

Table 1 summarizes the SE(Al,Na) and $SE(Al,Na)_{rel}$ of Al for Si at eight crystallographically non-equivalent T sites and the coordination states of Na^+ in the Na-MCM-22. It should be pointed out that the effective coordination of framework oxygen to Na^+ is limited to the Na^+–O^{2-} distance less than 2.73 Å [32]. Thus, Na^+ had a coordination number (CN) of 6 with five lattice oxygen in the 6-MR and one lattice oxygen in the $[4^3]$ unit (Table 1 and Fig. 3), and consequently did not cause a severe deformation of the D6 (Fig. 2C). That Na^+ was preferentially located at the positions close to 6-MR has been also found in the frameworks of Na-ZSM-5 [32], Na-FER [33] and Na-FAU [34] by the DFT calculations. The distance between Na^+ and the weighted mass center of the D6, denoted as r(Na. . .6-MR), was about 0.88 Å in the case of Al sited at T7 and T1 sites. With increasing SE(Al,Na), the r(Na. . .6-MR) increased, while the CN of Na^+ decreased.

Table 1 also shows the stable site notation of AlX-Na/Y with X and Y representing the T site for incorporating Al and the position for locating Na^+, respectively. The thermodynamically most favored Al7-Na/D6 and Al1-Na/D6 models indicates that the isomorphous substitution of Al for Si easily occurs at T7 and T1 sites with Na^+ located at the center of D6, as shown in Figs. 3 and 2C. Although the calculated energy difference between Al5-Na/D6, Al3-Na/HP6 or Al4-Na/D6 and Al7-Na/D6 is about 23–25 kJ/mol, one may expect that Al could also occupy T5, T3 and T4 sites. This has been found in ZSM-5, TS-1 and FAU zeolites [14,27,35,36]. This is because that some other factors also affect the Al locations, e.g. (*i*) the differences in kinetic limitations for inserting Al in crystallographically distinct lattice sites; (*ii*) the role of template and water molecules during synthesis of MCM-22; (*iii*) Na^+ is present in the hydrated form; (*iv*) the thermodynamic stability of formed Al-substituted subunits which might be suitable for incorporation of Al only in certain lattice sites; (*v*) the thermodynamic stability of as-synthesized product, which contains template and water molecules.

As discussed above, the most possible sites for accommodating Al in the framework of Na-MCM-22 are T7 and T1, followed by T5, T3 and T4, while T2, T8 and T6 sites are very unstable when Al is incorporated. The unit cell of the MWW structure contains 12 × T1, 12 × T2, 12 × T3, 12 × T4, 12 × T5, 4 × T6, 4 × T7 and 4 × T8 sites. Three T1 sites link to one T7 site and one T6 site to form one $[4^3]$ unit. Thus, 4 $[4^3]$ units are present in one unit cell (Figs. 1 and 4). Taking the site multiplicity into account, T7 and T1 sites might be equally occupied by Al, since the SE(Al,Na) of Al for Si at T7 site is about 4 kJ mol^{-1} lower than that at T1 site and the template and water molecules play an important role in the crystallization of MCM-22. As shown in Fig. 1, T1 sites are connected to T7 via one oxygen atom, making the simultaneous incorporation of Al in these

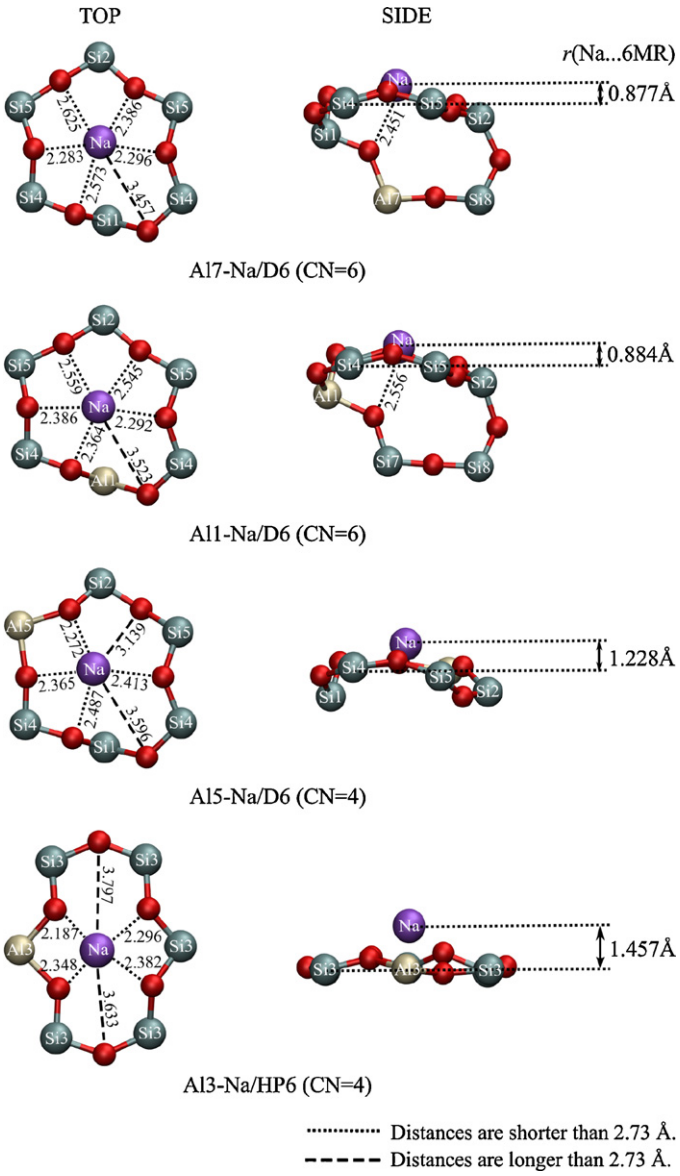

Fig. 3. Schemes for top and side views of the selected stable Na-MCM-22 structures.

two adjacent T sites impossible according to the Löwenstein's rule [37]. In addition, Next-Nearest-Neighbor sites of Al1–O–Si–O–Al1 (NNN species) [38] would be also very difficult to form because the occupation of two or three T1 sites by Al in one small $[4^3]$ unit would result in high density of negative charges, consequently, making the $[4^3]$ unit unstable. This is in line with the finding made by Čejka et al. [5,39], who reported that more than 70% of Al atoms were present as $((Si–O)_{n\geq 3}–Al–(Si–O)_{n\geq 3})$ species in the framework of MCM-22. Thus, it can be deduced that only four T7 and T1 sites would be occupied by Al per unit cell. As we know, Na-MCM-22 is generally synthesized with the synthesis gel having a Si/Al ratio of 10–20 [5,6,11,14,40,41], showing that one unit cell would have 6.5–3.4 Al atoms if all the Al species in the synthesis gel are incorporated in the framework. For the synthesis gel with a Si/Al ratio smaller than 17, Al would also occupy T5, T3 and T4 sites (the second group of Table 1) besides four sites of T7 and T1. It should be noted that this does not exclude the possibility of incorporation of Al in T5, T3 and T4 sites when the Si/Al ratio is larger than 17. Since there are many factors, such as kinetic limitation and role of template and water molecules, affecting the Al location in the framework, it might be only to say that the probability of Al occu-

(A) T7 and T1 Sites Per Unit Cell

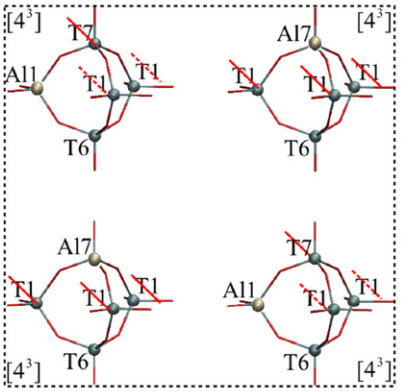

(B) Connectivity Matrix

	T7	T1	T5	T3	T4
T7	5N	2N	4N[a]	4N[b]	3N[a]
T1	2N	3N	3N[a]	5N	2N
T5	4N[a]	3N[a]	2N	3N	2N
T3	4N[b]	5N	3N	2N	4N
T4	3N[a]	2N	2N	4N	2N

2N: NN site, Al–O–Al linkage
3N: NNN site, Al–O–Si–O–Al linkage
4N: NNNN site, Al–O–$(Si–O)_2$–Al linkage
5N: NNNNN site, Al–O–$(Si–O)_3$–Al linkage
a: Two T sites are both in the DOH cage
b: Two T sites are located in different channel

Fig. 4. (A) Schemes for possible configurations of four Al atoms sited at T1 and T7 sites; (B) connectivity matrix of T sites in the first two groups of Table 1.

pying at T5, T3 and T4 sites is significantly smaller than in T7 and T1.

It can be seen from Fig. 4 that both T5 and T4 sites could form NNN and NNNN species (Al–O–$(Si–O)_{n=1,2}$–Al) with T1 or T7 in the modified DOH cage (Figs. 2 and 4). As discussed above, the formation of NNN and NNNN species in one small cage is unfavorable because of high negative charge density. Thus, the possibility for insertion of Al in T5 and T4 sites would be smaller than that in T3 sites. T3 sites are located at both the 10S and the HP, and consequently far from T1 sites, causing Al to exist mainly as an isolated state. T3 might stably form NNNN species with T7 because these two sites are positioned at different secondary structure units, and hence, with low negative charge density and low *SE*(Al,Na). Therefore, T3 sites are more favorable for accommodation of Al than T5 and T4 when T1 or T7 sites have been occupied by Al atoms. Thus, the probability of Al in eight crystallographically distinct lattice sites decreased in the order: T7 ≈ T1 > T3 > T5 > T4 > T2 > T8 > T6.

3.2. Location of bridging OH species in H-MCM-22

The isomorphous substitution of Al(III) for Si(IV) introduces negative charges in its framework. These negative charges are mostly compensated by Na^+ ions, as supported by the fact that no Brönsted acid sites could be detected in Na-MCM-22. The ion-exchange of Na^+ with NH_4^+ and the following calcination produce proton counter-ions. These protons would be located at the positions near the oxygen atoms bonding to Al and generate Brönsted acid sites. It should be pointed out that the positions of Al in the framework cannot be altered during the ion-exchange and calcination processes, but the generated H^+ would move around Al if the geometric space allows this movement.

The *SE*(Al,H) is used here as a measure of the stability of Brönsted acid sites. The lower the *SE*(Al,H) is, the more stable the Al–OH–Si site is. Table 2 shows the *SE*(Al,H) and the $SE(Al,H)_{rel}$ of 13 different Al–OH–Si species with the exception of Al7–O5H–Si8, the formation of which would cause the collapse of zeolite framework because its T–O–T angle is 180° based on the average symmetry obtained from XRD measurement [2,18]. It is clear that the *SE*(Al,H) of Al7–O4H–Si1 was the lowest, followed by that of Al1–O4H–Si7. This shows that H is bonded to O4 when Al is located at the preferential sites of T7 and T1, and that the *SE*(Al,H) is highly dependent on the sitings of Al in the framework. The bridging OH species with Al located at the preferential sites gave low *SE*(Al,H). In addition, the formation of hydrogen bond also decreased the *SE*(Al,H) (Table 2) although the decrease degree was related to the position of O(2) atom in the hydrogen bond of O(1)–H···O(2). As a result, Al5–O6H–Si4, Al5–O9H–Si2, Al4–O3H–Si1, Al4–O6H–Si5 and Al1–O2H–Si6 species showed smaller *SE*(Al,H) than Al3–O12H–Si3, while Al3–O11H–Si2 and Al5–O8H–Si5 exhibited a *SE*(Al,H) similar to that of Al3–O12H–Si3 (Table 2).

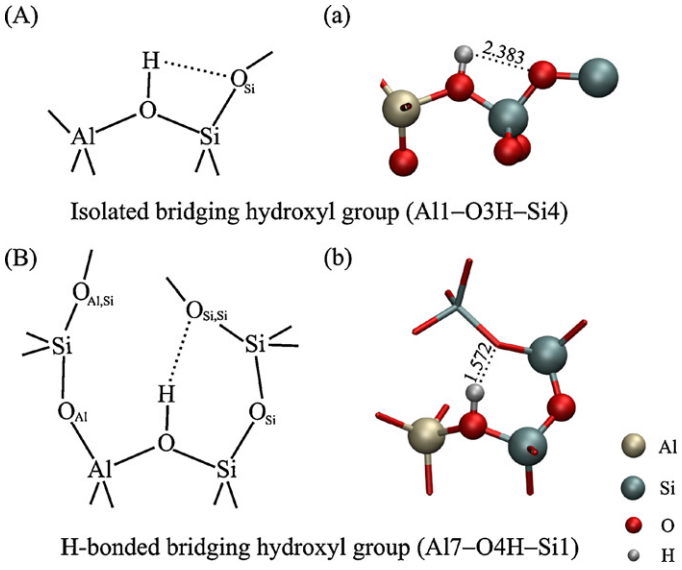

Fig. 5. Schemes for the most stable isolated and H-bonded bridging OH species.

Two different bridging OH species, viz. H-bonded and isolated bridging OH species, are present in H-MCM-22 (Table 2 and Fig. 5). This is in agreement with that observed in H-ZSM-5 by Sillar and Burk [42–44]. For the H-bonded bridging OH species, the proton is stabilized by hydrogen bonding to one neighboring lattice oxygen atom. This type of bridging OH species could be more easily formed in H-MCM-22 than in H-ZSM-5 owing to the presence of $\{4^35^66^3[4^3]\}$ cages in the framework. The $\{4^35^66^3[4^3]\}$ is a DOH cage modified with a reversed –T–O–T– chain which passes through the center with the two T atoms residing on the 3-fold axis, as

Table 2
Calculated SE(Al,H) (kJ mol^{-1}), $SE(Al,H)_{rel}$ (the substitution energy relative to that of Al7–O4H–Si1, kJ mol^{-1}) and geometry parameters (Å) of various Al–OH–Si species in H-MCM-22.

Al–OH–Si	Models	SE(Al,H)	$SE(Al,H)_{rel}$	r(O–H) r(Al–O) r(Si–O)	$r(H\cdots O_{Al})$ $r(H\cdots O_{Si})$ $r(H\cdots O_{Al,Si})$ $r(H\cdots O_{Si,Si})$[a]
Al7–O4H–Si1	8T:21T:89T	−171.2	0.0	1.009 1.917 1.725	3.025 2.609 4.384 1.572[H]
Al1–O4H–Si7	8T:21T:89T	−146.1	25.0	1.017 1.968 1.698	2.708 2.914 1.548[H] 3.997
Al5–O6H–Si4	8T:24T:83T	−145.7	25.4	1.004 1.861 1.679	2.687 2.604 2.855 1.572[H]
Al5–O9H–Si2	8T:23T:94T	−141.4	29.7	0.978 1.901 1.688	2.739 2.671 4.016 1.974[H]
Al4–O3H–Si1	8T:21T:82T	−126.7	44.5	0.972 1.892 1.659	2.078[H] 2.890
Al4–O6H–Si5	8T:24T:83T	−124.1	47.1	1.024 1.873 1.672	2.719 2.685 1.504[H] 2.789
Al1–O2H–Si6	8T:21T:89T	−123.2	48.0	0.993 1.888 1.683	3.130 2.673 1.785[H] 5.388
Al1–O3H–Si4	8T:21T:82T	−122.6	48.6	0.967 1.846 1.674	2.727 2.383[I]
Al3–O11H–Si2	8T:16T:91T	−114.4	56.8	1.019 1.870 1.660	2.495 2.741 1.554[H] 2.781
Al5–O8H–Si5	8T:20T:88T	−113.6	57.6	0.996 1.904 1.689	2.369 2.532 3.109 1.675[H]
Al3–O12H–Si3	8T:19T:94T	−112.2	59.0	0.970 1.919 1.701	2.784[I] 2.840
Al3–O13H–Si3	8T:24T:83T	−107.0	64.1	0.968 1.912 1.696	2.729 2.590[I]
Al4–O7H–Si4	8T:22T:80T	−92.9	78.2	0.968 1.961 1.711	2.763[I] 2.897

[a] Oxygen atoms are labeled in Fig. 5(B).
[H] H-bonded bridging OH species.
[I] Isolated bridging OH species.

shown in Fig. 2. This unusual connectivity is completed by putting a TO_3 cap on the top of the cage, and thereby, forming a small [4^3] unit. The hydrogen bonds (O–H···O) in H-MCM-22 were formed between the [4^3] units and the 6-MR of DOH cages with the bridging OH species located inside the DOH cages (Fig. 3). They have a shorter H···O distance than those present in H-ZSM-5. The smallest H···O distance was 1.504 Å for the Al4–O6H–Si5 species in the DOH cage, while it was 1.762 Å for the H-ZSM-5 [43]. The hydrogen bonds stabilized the bridging OH species of Al7–O4H–Si1, Al1–O4H–Si7 and Al5–O6H–Si4 by about 18–21 kJ mol^{-1} [43], making the protons of these bridging OH species unable to act as Brönsted acid sites, as supposed by Sastre et al. [14].

In the case of isolated bridging OH species, one H atom is bonded to one oxygen atom. The distances of these hydrogen atoms to the nearest oxygen atoms were in the range of 2.383–2.784 Å (r(H···O) in Table 2). The stable isolated bridging OH species in H-MCM-22 were Al1–O3H–Si4, Al3–O12H–Si3, Al3–O13H–Si3 and Al4–O7H–Si4. It should be mentioned that the O12 and O13 are different siting positions for H atoms although they both share the same substitution site of T3 (Fig. 1). The protons of these isolated bridging OH species extended in the 10-MR channels with the exception that the proton of Al3–O12H–Si3 pointed to the 6-MR of HP. Therefore, these protons interacted solely with their attached lattice oxygen atoms, and consequently, easily transferred to reactant species, giving rise to Brönsted acidity. In contrast, the H-bonded bridging OH species are more stable than the isolated ones, leading to difficulty in cleaving the O–H bond and showing weak acidity.

3.3. O–H stretching vibration frequencies

Study of the Brönsted acidity of H-MCM-22 has received much attention because of the presence of 8 crystallographically different lattice sites in its framework. Corma et al. [10] reported that two types of isolated bridging OH species were present in H-MCM-22 as they observed two absorbance bands at 3620 and 3575 cm^{-1} in its OH-region IR spectra. Onida et al. [11] further deconvolved the 3620 cm^{-1} band into two components at 3628 and 3618 cm^{-1}, and attributed them to two types of isolated bridging OH species probably located in the supercages and in the 10-MR channels, respectively. Recently, these three types of isolated Si(OH)Al species were also observed together with the H-bonded bridging OH species located at the HP, which exhibits a broad absorbance band around 3375 cm^{-1}, by Bevilacqua et al. [13].

The calculated vibrational frequencies of bridging OH species are summarized in Table 3. A linear relationship was observed between anharmonic frequencies (ω_{OH}) and O–H distances. The anharmonic frequencies (ω_{OH}) proportionally decreased with increasing O–H distances [45], showing that the stretching frequency of the OH species is highly dependent on its bond strength.

The anharmonic frequencies shown in Table 3 can be divided into two groups. The first group is due to the isolated bridging OH species, whereas the second group corresponds to the H-bonded bridging OH species. The anharmonic frequencies of the Al1–O3H–Si4, Al3–O13H–Si3 and Al4–O7H–Si4 species in the first group were 3628 ± 6, 3597 ± 4 and 3592 ± 4 cm^{-1}, respectively. It should be first pointed out that the formation of these three isolated bridging OH species is possible due to the proton hopping. Although the acidic proton is usually bonded to one of the four oxygen atoms surrounding the negatively charged Al, it can jump from one oxygen ion to another one, and its mobility is significantly increased by heating or H_2O molecules [16,46]. Thus, it could be deduced that these three species are probably responsible for the absorbance bands observed at 3628 and 3600 cm^{-1} in the OH-region IR spectrum of H-MCM-22. Table 3 shows that the OH species corresponding to these two bands were located at Su12 and 10S, being consistent with the results obtained by many researchers [10,11,13]. In the transformation of *m*-xylene over H-MCM-22, it was found that the 3620 cm^{-1} band decreased by about 75% in intensity when the sample completely deactivated, which indicates that about 75% of the inner acid sites would be located at or accessible via the T1-, T4- and T5-containing supercages [8,47]. The absorbance band at 3628 cm^{-1} is the most intense in the OH-region IR spectrum of H-MCM-22. This implies that abundant zeolitic OH species contribute to this frequency [13,18], which, as expected, coincides well with the Al1–O3H–Si4 species. As shown above, T1 site is one of the most favorable positions for accommodating Al; therefore, much more Al would be incorporated in T1 sites than in T3 and T4. The anharmonic frequency of Al3–O12H–Si3 species with the proton sited in HP was 3574 ± 3 cm^{-1}. This species should correspond to the observed 3575 cm^{-1} band, proving the surmise of Bevilacqua et al. [13] that the OH species contributing to this band might be located at the O12 position. It is worth noting that the bridging Al7–OH–Si species are not possible to be observed because Na^+ bonding to Al7–O^-–Si species cannot be exchanged with NH_4^+ due to the steric constraint.

The stretching vibration frequencies of the H-bonded bridging OH species were in the range of 3401 ± 1–2575 ± 6 cm^{-1}, exhibiting a broad absorbance band around 3375 cm^{-1} in the OH-region IR spectrum. Bevilacqua et al. supposed that this band was attributed to internal H-bonded OH species possibly located at inaccessible O4 positions [13]. Indeed, Table 2 shows that Al7–O4H–Si1,

Table 3
Comparison of calculated anharmonic O–H vibration stretching frequencies (ω_{OH}, cm^{-1}) and geometry parameters (Å) of various Al–OH–Si species in H-MCM-22 with the reported IR-measured and calculated O–H vibration stretching frequencies.

Al–OH–Si	r(O–H)	r(O–H O)[a]	Proton pointing to	$2x_e\omega_{eOH}$[b]	ω_{OH}[c]	Expt. values	Reported cal. frequencies
Al1–O3H–Si4	0.967	2.383	Su	187.0	3628 ± 6	3622 [14]; 3625–3618 (Su) [13]; 3628 (Su) [11]	3616 [16]; 3628 [18]
Al3–O13H–Si3	0.968	2.590	10S	195.1	3597 ± 4	3618–3600 (10S) [13]; 3618 (10-MR channel) [11]	–
Al4–O7H–Si4	0.968	2.763	Su	194.1	3592 ± 4	3618-3600 (10S) [13]; 3618 (10-MR channel) [11]	–
Al3–O12H–Si3	0.970	2.522	HP	201.2	3574 ± 3	3575 [10]; 3575 (O12) [13]; 3576 [14]; 3585 (HP) [11]	–
Al5–O9H–Si2	0.978	1.974	Su	229.7	3401 ± 1	A broad band around 3375 [13]	3458 [18]; 3605 [16]
Al1–O2H–Si6	0.993	1.785	10C	294.0	3115 ± 2		–
Al5–O8H–Si5	0.996	1.675	Su	317.8	3016 ± 0		–
Al5–O6H–Si4	1.004	1.572	Su	382.5	2853 ± 5		–
Al7–O4H–Si1	1.009	1.572	Su	355.7	2814 ± 1		–
Al1–O4H–Si7	1.017	1.478	Su	462.0	2575 ± 6		–

[a] The distance of r(O–H···O) is the same as the r(H···O) in Table 2 labeled by *H* or *I*.
[b] ω_{eOH} is harmonic frequency (cm^{-1}), x_e is the anharmonic constant.
[c] ω_{OH} is anharmonic frequency (cm^{-1}) including the standard deviation (cm^{-1}) of the calculated points from the Morse curve (1 hartree = 2.1947×10^{-5} cm^{-1}).

Table 4
Calculated adsorption energies (kJ mol^{-1}) of N_2 and CO molecules on the Brönsted acid sites and geometric parameters (Å) of N_2- and CO-adsorbed H-MCM-22.

Al–OH–Si	H-MCM-22	N_2-MCM-22			CO-MCM-22		
	r(O–H)	r′(O–H)	r′(N···H)	E_{ads}[a]	r′(O–H)	r′(C···H)	E_{ads}[a]
Al3–O13H–Si3	0.968	0.975	2.066	−17.3	0.989	1.911	−24.9
Al4–O7H–Si4	0.968	0.977	1.864	−18.4	0.985	1.917	−21.9
Al1–O3H–Si4	0.967	0.975	1.972	−12.5	0.986	1.938	−18.7
Al3–O12H–Si3	0.970	0.972	2.049	−9.8	0.983	1.902	−15.6

[a] With ZPE and BSSE corrections calculated at corresponding ONIOM model systems.

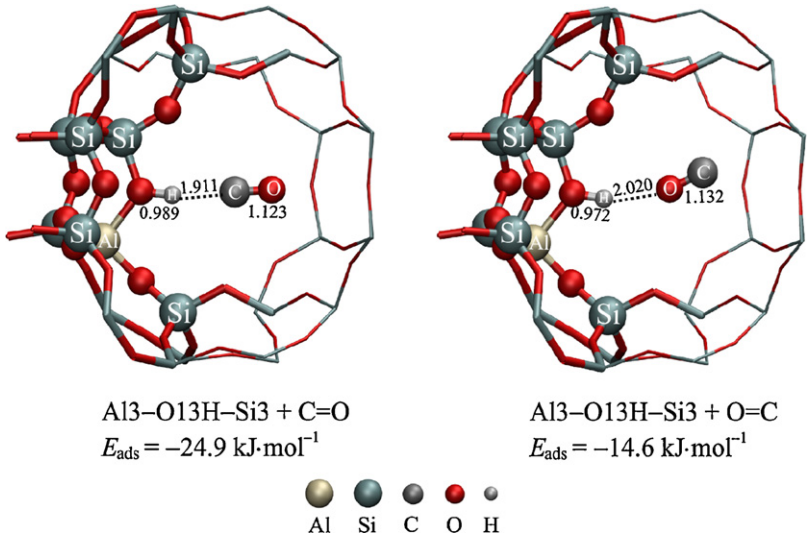

Fig. 6. Optimized structures of CO adsorption on the Brönsted acid sites (Al3–O13H–Si3) via the C atom and via the O atom.

Al1–O4H–Si7, Al5–O6H–Si4 and Al4–O6H–Si5 species all formed O4-containing hydrogen bonds. For comparison, the IR-measured and the calculated OH stretching vibration frequencies reported in literatures are also listed in Table 3. Clearly, this work gave more accurate values than the previous ones [16,18].

3.4. Brönsted acidity

The acid strength of different types of bridging OH species was studied by calculating the adsorption energies of small basic N_2 and CO molecules on these OH species. The adsorption energy (E_{ads}) is defined as the energy difference of the adsorption complexes (Z–OH···B) and the two monomers (Al–OH–Si (denoted as Z–OH) species and probe molecule B (N_2 or CO)) (Eq. (3)). The zero-point energy (ZPE) and basis set superposition errors (BSSE) were also included. According to the Eq. (3), the more negative the E_{ads}, the stronger the interaction between Z–OH and B; consequently, the stronger the acidity of Z–OH. Because of the weak acidity of H-bonded bridging OH species [13,48], the adsorption energies of N_2 and CO on the isolated bridging OH species are calculated here (Table 4).

$$E_{ads} = E(\text{Z–OH}\cdots\text{B}) - [E(\text{Z–OH}) + E(\text{B})] \quad (3)$$

3.4.1. Interaction with nitrogen

Table 4 shows that Al3–O13H–Si3, Al4–O7H–Si4, Al1–O3H–Si4 and Al3–O12H–Si3 sites exhibited N_2 adsorption energies of–17.3,–18.4,–12.5 and–9.8 kJ mol^{-1}, respectively. This is indicative of the existence of interaction between N_2 molecule and all the four bridging OH species, and consequently, leading to a slight elongation of the O–H bond. The more negative E_{ads} of N_2 on the Al3–O13H–Si3, the Al4–O7H–Si4 and the Al1–O3H–Si4 sites than that on the Al3–O12H–Si3 site show that the former three bridging OH species exhibited stronger Brönsted acidity than the latter one.

3.4.2. Interaction with carbon monoxide

CO is also often used as a probe molecule to study the acidity of zeolites because of its sensitivity of the stretching mode to the features of surface sites. Fig. 6 shows that the adsorption of CO on the Brönsted acid sites via the C atom was more stable than that via the O atom. Table 4 lists the calculated E_{ads} of CO on different Brönsted acid sites. Clearly, the E_{ads} of CO on the Al3–O13H–Si3 and Al4–O7H–Si4 sites are higher than those on the Al1–O3H–Si4 and Al3–O12H–Si3 sites, indicating CO adsorption on Al3–O13H–Si3 and Al4–O7H–Si4 sites is stronger than on Al1–O3H–Si4 and Al3–O12H–Si3 sites, in agreement with the results obtained by Onida et al. [11], who reported that CO molecules might have a weak interaction with the acid sites located in the HP. Consequently the isolated Al3–O13H–Si3 and Al4–O7H–Si4 species with proton pointing to the 10S and 10C respectively show stronger Brönsted acidity than Al1–O3H–Si4 and Al3–O12H–Si3. The former two bridging OH species gave the absorbance band at 3600 cm^{-1}, whereas the latter two displayed the bands at 3628 and 3575 cm^{-1}, respectively. This shows that the OH frequencies calculated by the ONIOM method in this work coincide well with those observed by IR spectroscopy [11,13,14].

4. Conclusions

The locations of Al atoms and Brönsted acid sites in the framework of MCM-22 were calculated by using the ONIOM method. The strengths of different Brönsted acid sites were evaluated.

Based on the optimized Na-MCM-22 model, the thermodynamically most favorable sites for accommodation of Al are T7 and T1 sites, followed by T3, T5 and T4, while T2, T8 and T6 sites are much higher in energy when Al is incorporated. Na^+ is preferentially sited at the 6-MR of the modified DOH cage by hexa-bonding to vicinal lattice oxygen atoms without significantly deforming the 6-MR. There are two different types of bridging hydroxyl groups in H-MCM-22, viz. isolated and H-bonded Si(OH)Al species. The preferential location of Al at T1 sites give the most intense absorbance band at 3628 ± 6 cm^{-1} in the OH-region IR spectrum of H-MCM-22, whereas Al3–O13H–Si3, Al4–O7H–Si4 and Al3–O12H–Si3 species show absorbance bands at 3597 ± 4, 3592 ± 4 and 3574 ± 3 cm^{-1}, respectively. These three bands correspond to the observed weak absorbance bands at 3600 and 3575 cm^{-1} due to insertion of a small number of Al atoms in T3 and T4 sites. The O–H stretching vibration frequencies of H-bonded bridging OH species were in the range from 3401 ± 1 to 2575 ± 6 cm^{-1}, giving a broad absorbance band at 3375 cm^{-1} in the IR spectrum. The adsorption energies of N_2 and CO on the isolated bridging OH species show that the Al3–O13H–Si3 and Al4–O7H–Si4 species with protons pointing to the 10S and 10C exhibited stronger Brönsted acidity than Al1–O3H–Si4 and Al3–O12H–Si3.

Acknowledgements

This work is supported by the National Science Foundation of China (Nos. 20876163 and 20773153), National Basic Research Program of China (Nos. 2009CB226101, 2010CB234603 and 2011CB201403), Sino-Australia bilateral cooperation program (No. 2007DFC60110) and "Hundred of Talents" project of Chinese Academy of Sciences. T. T. thanks the support of the Ministry of Education, Culture, Science and Technology of Japan.

References

[1] A. Corma, A. Martínez, Catal. Rev. 35 (1993) 483–570.
[2] M.E. Leonowicz, J.A. Lawton, S.L. Lawton, M.K. Rubin, Science 264 (1994) 1910–1913.
[3] A. Corma, U. Diaz, V. Fornés, J.M. Guil, J. Martínez-Triguero, E.J. Creyghton, J. Catal. 191 (2000) 218–224.
[4] D. Vuono, L. Pasqua, F. Testa, R. Aiello, A. Fonseca, T.I. Koranyi, J.B. Nagy, Micropor. Mesopor. Mater. 97 (2006) 78–87.
[5] J. Dědeček, J. Čejka, M. Oberlinger, S. Ernst, Stud. Surf. Sci. Catal. 142 (2002) 23–30.
[6] K. Góra-Marek, J. Datka, Stud. Surf. Sci. Catal. 158A (2005) 837–844.
[7] S. Hong, H. Min, C. Shin, P. Cox, S. Warrender, P. Wright, J. Am. Chem. Soc. 129 (2007) 10870–10885.
[8] J. Rigoreau, S. Laforge, N. Gnep, M. Guisnet, J. Catal. 236 (2005) 45–54.
[9] H.K. Min, M.B. Park, S.B. Hong, J. Catal. 271 (2010) 186–194.
[10] A. Corma, C. Corell, V. Fornés, W. Kolodziejski, J. Pérez-Pariente, Zeolites 15 (1995) 576–582.
[11] B. Onida, F. Geobaldo, F. Testa, F. Crea, E. Garrone, Micropor. Mesopor. Mater. 30 (1999) 119–127.
[12] D. Ma, F. Deng, R. Fu, X. Han, X. Bao, J. Phys. Chem. B 105 (2001) 1770–1779.
[13] M. Bevilacqua, D. Meloni, F. Sini, R. Monaci, T. Montanari, G. Busca, J. Phys. Chem. C 112 (2008) 9023–9033.
[14] G. Sastre, V. Fornes, A. Corma, J. Phys. Chem. B 104 (2000) 4349–4354.
[15] Y. Wang, J. Zhuang, G. Yang, D. Zhou, D. Ma, X. Han, X. Bao, J. Phys. Chem. B 108 (2004) 1386–1391.
[16] Y. Wang, D. Zhou, G. Yang, X. Liu, D. Ma, D. Liang, X. Bao, Chem. Phys. Lett. 388 (2004) 363–366.
[17] A. Zheng, L. Chen, J. Yang, M. Zhang, Y. Su, Y. Yue, C. Ye, F. Deng, J. Phys. Chem. B 109 (2005) 24273–24279.
[18] D. Zhou, Y. Bao, M. Yang, N. He, G. Yang, J. Mol. Catal. A: Chem. 244 (2006) 11–19.
[19] Y. Li, W. Guo, S. Yuan, W. Fan, J. Wang, H. Jiao, J. Mol. Struct. (Theochem.) 916 (2009) 53–60.
[20] S. Lee, C. Shin, D. Yang, S. Ahn, I. Nam, S.B. Hong, Micropor. Mesopor. Mater. 68 (2004) 97–104.
[21] A.F. Wells, Structural Inorganic Chemistry, 5th ed., Oxford University Press, New York, 1984, p. 326.
[22] P. Simoncic, T. Armbruster, Am. Miner. 89 (2004) 421–431.
[23] R. Bulaĭnek, I. Voleskaĭ, E. Ivanova, K. Hadjiivanov, P. Nachtigall, J. Phys. Chem. C 113 (2009) 11066–11076.
[24] D. Nachtigallovaĭ, P. Nachtigall, J. Sauer, Phys. Chem. Chem. Phys. 3 (2001) 1552–1559.
[25] V.D. Dominguez-Soria, P. Calaminici, A. Goursot, J. Chem. Phys. 127 (2007) 154710–154718.
[26] Ch. Baerlocher, L.B. McCusker, D.H. Olson, Altas of Zeolite Framework Types, 6th ed., Elsevier, Amsterdam, 2007, p. 234.
[27] R. Deka, V. Nasluzov, E.A. Ivanova Shor, A. Shor, G. Vayssilov, N. Rösch, J. Phys. Chem. B 109 (2005) 24304–24310.
[28] X. Solans-Monfort, M. Sodupe, V. Branchadell, J. Sauer, R. Orlando, P. Ugliengo, J. Phys. Chem. C 109 (2005) 3539–3545.
[29] M.J. Frisch, G.W. Trucks, H.B. Schlegel, G.E. Scuseria, M.A. Robb, J.R. Cheeseman Jr.J.A., T. Montgomery, K.N. Vreven, J.C. Kudin, J.M. Burant, S.S. Millam, J. Iyengar, V. Tomasi, B. Barone, M. Mennucci, G. Cossi, N. Scalmani, G.A. Rega, H. Petersson, M. Nakatsuji, M. Hada, K. Ehara, R. Toyota, J. Fukuda, M. Hasegawa, T. Ishida, Y. Nakajima, O. Honda, H. Kitao, M. Nakai, X. Klene, J.E. Li, H.P. Knox, J.B. Hratchian, V. Cross, C. Bakken, J. Adamo, R. Jaramillo, R.E. Gomperts, O. Stratmann, A.J. Yazyev, R. Austin, C. Cammi, J.W. Pomelli, P.Y. Ochterski, K. Ayala, G.A. Morokuma, P. Voth, J.J. Salvador, V.G. Dannenberg, S. Zakrzewski, A.D. Dapprich, M.C. Daniels, O. Strain, D.K. Farkas, A.D. Malick, K. Rabuck, J.B. Raghavachari, J.V. Foresman, Q. Ortiz, A.G. Cui, S. Baboul, J. Clifford, B.B. Cioslowski, G. Stefanov, A. Liu, P. Liashenko, I. Piskorz, R.L. Komaromi, D.J. Martin, T. Fox, M.A. Keith, C.Y. Al-Laham, A. Peng, M. Nanayakkara, P.M.W. Challacombe, B. Gill, W. Johnson, M.W. Chen, C. Wong, J.A. Gonzalez, Pople Gaussian 03 (Revision E.01), Gaussian, Inc., Wallingford, CT, 2004.
[30] V.G. IL'in, N.V. Turutina, V.N. Solomakha, Stud. Surf. Sci. Catal. 49A (1989) 345–353.
[31] R.R. Xu, W.Q. Pang, J.H. Yu, Q.S. Huo, J.S. Chen, Chemistry-Zeolites and Porous Materials, Scientific Press of China, Beijing, 2004, p. 382 (in Chinese).
[32] J. Kučera, P. Nachtigall, Phys. Chem. Chem. Phys. 5 (2003) 3311–3317.
[33] C. Areán, G. Palomino, E. Garrone, D. Nachtigallová, P. Nachtigall, J. Phys. Chem. B 110 (2006) 395–402.
[34] G.N. Vayssilov, M. Staufer, T. Belling, K.M. Neyman, H. Knözinger, N. Rösch, J. Phys. Chem. B 103 (1999) 7920–7928.
[35] D. Nachtigallovaĭ, P. Nachtigall, M. Sierka, J. Sauer, Phys. Chem. Chem. Phys. 1 (1999) 2019–2026.
[36] U. Eichler, M. Brändle, J. Sauer, J. Phys. Chem. B 101 (1997) 10035–10050.
[37] W. Löwenstein, Am. Miner. 39 (1954) 92–96.

[38] L.A. Pine, P.J. Maher, W.A. Wachter, J. Catal. 85 (1984) 466–476.
[39] J. Čejka, J. Dědeček, J. Kotrla, M. Tudor, N. Žilková, S. Ernst, Stud. Surf. Sci. Catal. 135 (2001) 352.
[40] K. Okumura, M. Hashimoto, T. Mimura, M. Niwa, J. Catal. 206 (2002) 23–28.
[41] A. Abraham, S.B. Hong, R. Prins, J.A. van Bokhoven, Stud. Surf. Sci. Catal. 158 (2005) 679–686.
[42] V.L. Zholobenko, L.M. Kustov, V.Yu. Borovkov, V.B. Kazansky, Zeolites 8 (1988) 175–178.
[43] K. Sillar, P. Burk, J. Phys. Chem. B 108 (2004) 9893–9899.
[44] C. Callam, S. Singer, T. Lowary, C. Hadad, J. Am. Chem. Soc. 123 (2001) 11743–11754.
[45] C. Chizallet, G. Costentin, M. Che, F. Delbecq, P. Sautet, J. Am. Chem. Soc. 129 (2007) 6442–6452.
[46] R.Q. Albuquerque, G. Calzaferri, Chem. Eur. J. 13 (2007) 8939–8952.
[47] S. Laforge, D. Martin, M. Guisnet, Micropor. Mesopor. Mater. 67 (2004) 235–244.
[48] K. Sillar, P. Burk, Chem. Phys. Lett. 393 (2004) 285–289.